applied optics

Visualization of the influence of the air conditioning system to the high-power laser beam quality with the modulation coherent imaging method

Hua Tao,[1] Suhas P. Veetil,[2] Xingchen Pan,[1] Cheng Liu,[1,*] and Jianqiang Zhu[1]

[1]Shanghai Institute of Optics and Fine Mechanics, Chinese Academy of Sciences, Shanghai 201800, China
[2]Department of Engineering Technology and Science, Higher Colleges of Technology, Fujairah 4114, United Arab Emirates
*Corresponding author: cheng.liu@hotmail.co.uk

Received 4 May 2015; revised 18 June 2015; accepted 19 June 2015; posted 19 June 2015 (Doc. ID 240229); published 21 July 2015

Air conditioning systems can lead to dynamic phase change in the laser beams of high-power laser facilities for the inertial confinement fusion, and this kind of phase change cannot be measured by most of the commonly employed Hartmann wavefront sensor or interferometry due to some uncontrollable factors, such as too large laser beam diameters and the limited space of the facility. It is demonstrated that this problem can be solved using a scheme based on modulation coherent imaging, and thus the influence of the air conditioning system on the performance of the high-power facility can be evaluated directly.

OCIS codes: (100.5070) Phase retrieval; (050.1970) Diffractive optics; (120.5050) Phase measurement; (070.0070) Fourier optics and signal processing.

http://dx.doi.org/10.1364/AO.54.006632

1. INTRODUCTION

High-power laser facilities employed in inertial confinement fusion (ICF) make use of laser beams having large diameters (tens of centimeters). The beam generated by the seed laser source passes through several large-diameter optical components during its transmission over several hundreds of meters before reaching the target [1]. In this process, certain factors, such as inaccuracies in material uniformity and surface profiles of large-diameter optical elements or the distortion that is introduced into the laser slabs when they are illuminated by the pulse of light from the flashlamps, seriously affect the quality of the transmitted beam and eventually lead to the failure of actual experiments [2–4]. So a strict control on the quality of the wavefront is required in ICF in order to focus a sufficiently high amount energy in the region of interest [5], and hence the monitoring of the phase of large-diameter laser beams becomes a task of great importance in the field of ICF. Air fluent or other environment vibrations are other kinds of important factors to influence phase distribution of the laser beams and then the performance of the whole facility. To keep the constant temperature and the high cleanliness in the whole building, the air conditioning system should work the whole day, and the generated air fluent and mechanical vibrations influence inevitably the laser beam stability and quality. Compared to static phase change due to the fabrication error of the optical element or material defects, which can be measured off-line, the dynamic phase change generated by the air conditioning system is more difficult to be measured accurately [2,6,7]. In theory Hartmann wavefront sensors can be applied to monitor this kind of dynamic phase change [8–11]. However, to shrink the diameter of the laser beam to the size of its sensor chip a complex and large beam shrinking device should be used. In addition, its resolution limited by its subaperture and the number of microlenses used is inadequate to meet the actual demand. Though a large-aperture interferometer used in conventional interferometry has enough accuracy and resolution [12], this method is practically not viable as it is challenging to provide enough space and stable enough environment for its element alignment and operation within the high-power facility. To estimate the influence of the air conditioning system the commonly adopted method was to observe the shifting of the focus spot or the change in near-field intensity distribution [13,14]. It is obvious that this method is too rough since the influence is directly on the phase and not on the intensity, and the phase change does not always lead to focus-spot shifting. There is a lack of a proper phase measurement device to monitor the dynamic phase change of the large-diameter laser beams and therefore the performance of the whole facility cannot be evaluated strictly.

In this paper we will demonstrate that the modulation coherent imaging (MCI) method, which was proposed in 2010 by Zhang and co-workers [15–17], can be used to evaluate the influence of the air conditioning system on the beam quality by measuring the laser beam phase change on-line. The MCI method uses only a piece of highly random phase plate (RPP) and a CCD camera and can retrieve the phase from one frame of intensity recorded, thus in comparison with coherent diffractive imaging (CDI) techniques that can also be used to measure the laser beam phase [18–21], MCI converges rapidly and is very compact in the structure and can be placed at any place within the facility to monitor the phase change of the laser beams. This is demonstrated by first recording diffraction patterns for a proper time in the initial stable environment when the air conditioning system is turned off, and then another set of diffraction patterns are recorded in a changing environment when the air conditioning is turned on and the air outlets are opened. The dynamic phase change of large-diameter laser beams can be retrieved by certain iterative calculations which may last only with one minute, and by comparing the phase change of three sets of experiments, the influence of the air conditioning system can be vividly observed and accurately evaluated.

2. BASIC PRINCIPLE OF MCI USED FOR DYNAMIC PHASE MEASUREMENT

Figure 1 shows the schematic of the MCI method. The sampling beam of a high-power laser is focused by a convergent lens and then illuminates a RPP near the focal plane. A CCD camera is kept at a certain distance from the RPP to record the diffraction patterns. The focal plane, the RPP plane, and the CCD camera plane are called the "entrance plane," the "modulator plane," and the "detector plane," respectively in the MCI algorithm. A constraint function, a circular aperture S_n is designed for the finite extent of the incident beam at the entrance plane. The modulator of the RPP has a known transmission function $O(x, y)$ that is designed in order to diffract the entrance wave into a large solid angle, yielding a flattened diffraction intensity pattern. Consequently, the requirements on the dynamic range of the detector are reduced. The reconstruction of the entrance wave function is done iteratively as follows, by taking a random initial guess for the entrance wave $\varphi_n(x, y)$ where n stands for the number of iterations:

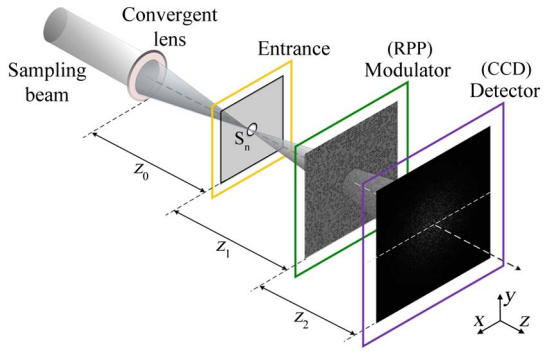

Fig. 1. Schematic of MCI method.

(i) The constraint function of circular aperture is $S_n = \begin{cases} 1, & 0 \le r \le r_n \\ 0, & r > r_n \end{cases}$ for the entrance plane, where r is the radius of the circular aperture. r_n $(n = 1)$ initially is a small constant of the order of micrometers. The exit wave function at the entrance plane is $\varphi_{e,n}(x, y) = \varphi_n(x, y) \cdot S_n$, where n represents the nth iteration.

(ii) Propagate $\varphi_{e,n}$ to the modulator plane, the entrance wave function at the modulator plane is $P_{m,n}(x, y) = \mathrm{FFT}[\varphi_{e,n}(x, y), z_1]$, in terms of the fast Fourier transform operator.

(iii) The exit wave function at the modulator plane is $\varphi_{m,n}(x, y) = P_{m,n}(x, y) \cdot O(x, y)$, where $O(x, y)$ is the transmittance function of the designed RPP.

(iv) Propagate the exit wave function to the detector plane. The wave function at the detector plane is $\phi_{m,n}(x, y) = \mathrm{FFT}[\varphi_{m,n}(x, y), z_2]$, where FFT represents Fourier propagation to a distance z_2 in the nth iteration.

(v) Replace the amplitude of the wave function obtained in step (iv) with the diffraction pattern intensity recorded by the CCD. The corrected wave function is now represented by $\phi_{c,n}(x, y) = \sqrt{I}\exp[i \arg|\phi_{m,n}(x, y)|]$, where I is the intensity of diffraction patterns recorded by the CCD and $\arg|\phi_{m,n}(x, y)|$ represents the phase of $\phi_{m,n}(x, y)$.

(vi) The wave function at the back side of the modulation plane is obtained as $\varphi_{c,n}(x, y) = \mathrm{FFT}^{-1}[\phi_{c,n}(x, y), z_2]$, where $\mathrm{FFT}^{-1}[\phi_{c,n}(x, y), z_2]$ represents Fourier backpropagation to a distance z_2 in the nth iteration.

(vii) Update the function

$$P_{\mathrm{new}}(x, y) = P_{m,n}(x, y) + \frac{|O(x, y)|}{|O(x, y)|_{\max}} \frac{O(x, y)^*}{[|O(x, y)|^2 + \alpha]} \times [\varphi_{c,n}(x, y) - P_{m,n}(x, y) \cdot O(x, y)],$$

where α is an appropriately chosen constant to suppress the noise [22].

(viii) Backpropagate $P_{\mathrm{new}}(x, y)$ to the entrance plane, the exit wave function at the entrance plane is $\varphi'_{e,n}(x, y) = \mathrm{FFT}^{-1}[P_{\mathrm{new}}(x, y), z_1]$, where $\mathrm{FFT}^{-1}[P_{\mathrm{new}}(x, y), z_1]$ represents Fourier backpropagation to a distance z_1 in the nth iteration.

(ix) Increase the value r_{n+1} about 0.1 μm in each iteration, update the exit wave function at the entrance plane as $\varphi_{e,n+1}(x, y) = \varphi'_{e,n}(x, y) \cdot S_{n+1}$.

(x) Repeat steps (i)–(ix) until the change between two successive iterations of the entrance wave $\varphi_{e,n}(x, y)$ becomes sufficiently small. The iteration is stopped in this case and the final wave functions obtained, $\varphi_{e,n}(x, y)$ and $P_{m,n}(x, y)$, are accurate distributions of the light field at the entrance and at the modulator plane. $P_{m,n}(x, y)$ is obtained as $P_{m,n}(x, y) = \mathrm{FFT}[\varphi_{e,n}(x, y), z_1]$.

We recorded diffraction patterns in the initial stable environment while the air conditioning system is turned off, and then recorded another set of diffraction patterns in a changing environment when the air conditioning is turned on and the air outlets are opened. We can now obtain the initial stable field $U(x', y')$ and the changing field $T(x', y')$ by numerically propagating the reconstructed wave functions present at the modulator plane, $P'_{m,n}(x, y)$ and $P''_{m,n}(x, y)$, to the plane exactly behind the condenser lens using the following Fresnel diffraction formula:

$$U(x',y') = \frac{\exp[ik(z_0+z_1)]}{i\lambda(z_0+z_1)} \times \iint P'_{m,n}(x,y)\exp\left[ik\frac{(x'-x)^2+(y'-y)^2}{2(z_0+z_1)}\right]\mathrm{d}x\mathrm{d}y,$$

$$T(x',y') = \frac{\exp[ik(z_0+z_1)]}{i\lambda(z_0+z_1)} \times \iint P''_{m,n}(x,y)\exp\left[ik\frac{(x'-x)^2+(y'-y)^2}{2(z_0+z_1)}\right]\mathrm{d}x\mathrm{d}y; \quad k = 2\pi/\lambda,$$

where λ is the wavelength of the sampling beam. The phase change occurring in the large-diameter laser beam can be obtained by calculating the phase of $U(x',y')T^*(x',y')$, where $T^*(x',y')$ is the conjugate of $T(x',y')$.

3. EXPERIMENT

The experimental setup is shown in Fig. 2. The high-power laser beam generated by the seed laser source propagates over several hundreds of meters and eventually reaches the target. In this high-power laser facility, the main air stream from the air conditioner blew to several parts of the facility including the front-end system, the preamplifier system, and the terminal target system. It also blew to the laser beam in the air and also some of the major optical components. The size of the outlet air stream is 100 cm × 60 cm and the estimated flow rate is about 0.8 m/s. Another quantitative factor to define the airflow is the supply air temperature. We kept the temperature at 22°C when the air conditioning system was turned on. The sample beam introduced by the sample mirror located before the final optics assembly, 12 cm in diameter and pulse duration of 1 s, is first reflected by a large reflecting mirror and then focused by an aspheric condenser lens with a focal length of 2750 mm. Since the measurement unit is to be placed in a limited space, the focused beam is reflected again by a smaller reflecting mirror to direct it to the RPP kept near the focal plane. The phase plate consists of an array of pixels that randomly take values of either 0 or π with the same probability. A computer is used for recording the diffraction patterns and a translation stage control is used while the extended ptychographical iterative engine (ePIE) algorithm is applied

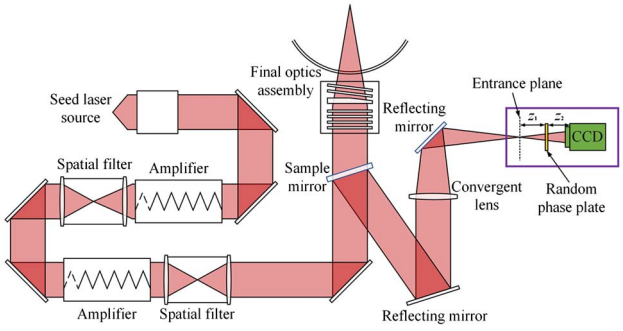

Fig. 2. Experimental setup for measuring the dynamic phase change of large-diameter laser beams in the high-power laser facility with MCI. The resulting diffraction patterns are recorded by a CCD.

to accurately measure the transmittance function $O(x,y)$ of the designed RPP [23,24]. A diffraction pattern is then recorded by a CCD camera behind the RPP. z_0 is the focal length of 2750 mm of the convergent lens. It is assumed that the CCD has $N \times N$ pixels, each of which are square and Δx_D in width. According to the Fresnel propagation algorithm, the sampling intervals at the modulator Δx_M and at the entrance plane Δx are related by $\Delta x_M = \lambda z_2/N\Delta x_D$; $\Delta x = \lambda z_1/N\Delta x_M = (z_1/z_2)\Delta x_D$, where λ is the wavelength of the laser source used. A diffraction pattern was calculated in the iterations with the following parameters: $\lambda = 1053$ nm; $z_1 = 80.3$ mm; $z_2 = 72.3$ mm; N = 2048; and $\Delta x_D = 18$ μm is in agreement with the experimental conditions. The CCD used is PIKE-421B (Allied Vision Technologies, AVT). The illuminating field on the RPP plane $P'_{m,n}(x,y)$ is then obtained from this diffraction pattern using the MCI method for the initial stable field. The air conditioning is then turned on and the air outlets are opened and another diffraction pattern is recorded by the CCD camera. The resulting illuminating field on the RPP plane $P''_{m,n}(x,y)$ is also obtained from this diffraction pattern with the same MCI method.

Figures 3(a) and 3(b) show the measured amplitude and phase distribution of the RPP with the ePIE algorithm, respectively. The phase distribution is either 0 or π represented in gray or black in the figure. Each cell size of the phase distribution is 18 μm × 18 μm and it is randomly distributed. This can effectively disperse the incident light beam and hence the dynamic range requirement of the detector can be reduced.

The diffraction pattern obtained in the initial stable field when the air conditioning system is turned off is shown in Fig. 4(a), where the obvious speckle is due to the random structure of the RPP. With the MCI algorithm, the focal plane distribution and the illumination on the modulator plane are reconstructed. Figure 4(b) shows the reconstructed amplitude distribution on the focal plane. Figures 4(c) and 4(d) show the reconstructed modulus and phase on the modulator plane, respectively. By propagating this numerically reconstructed field to the plane exactly behind the condenser lens, the amplitude and the phase of the illuminating field $U(x',y')$ are generated. Figures 4(e) and 4(f) show the amplitude and the phase of $U(x',y')$, respectively.

The results obtained by repeating the above steps in a changing environment when the air conditioning is turned on and the air outlets are opened are shown in Fig. 5. The detection and reconstruction procedures are repeated numerically to obtain the illuminating field $T(x',y')$. The recorded diffraction pattern is shown in Fig. 5(a) and the corresponding reconstructed amplitude distribution on the focal plane is shown in Fig. 5(b). The obvious change in the focus is due to a change in the initial environment while the air conditioning is turned on. Figures 5(c) and 5(d) show the amplitude and phase of the $P''_{m,n}(x,y)$, respectively. We obtain the transmitting function $T(x',y')$ by backpropagating $P''_{m,n}(x,y)$ to the plane exactly behind the condenser lens whose amplitude and phase distribution are shown in Figs. 5(e) and 5(f), respectively.

By calculating the phase of $U(x',y')T^*(x',y')$, the phase change that occurred in large-diameter laser beams is obtained

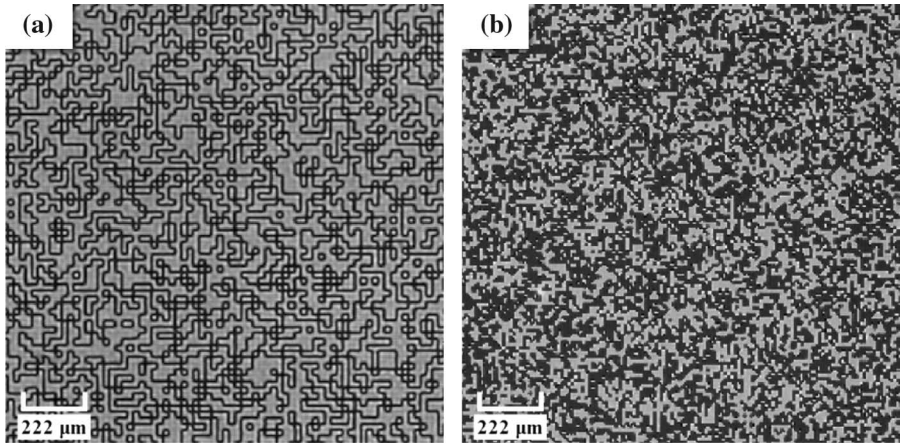

Fig. 3. (a) Amplitude and (b) phase distribution of $O(x, y)$ of the random phase plate (RPP) obtained with the ePIE algorithm.

by the proposed method. The amplitude distributions of $T(x', y')$ and the corresponding phase changes before the condenser lens were obtained from consecutive diffraction patterns recorded with a time interval of 1 s during the initial stable field when the air conditioning system is turned off. This is shown in Fig. 6. We notice that the amplitude distributions of $T(x', y')$ basically remain the same; however, there are some changes in phase but not very drastic. Figure 6(c) shows a phase distribution with values ranging from −0.7283 rad to −2.5180 rad in the initial stable field.

Figure 7 presents the amplitude distributions of $T(x', y')$ and corresponding phase changes before the condenser lens obtained from consecutive diffraction patterns recorded with a time interval of 1 s in a changing environment when the air conditioning is turned on and the air outlets are opened. Though only a minor change is observed for amplitude distributions of $T(x', y')$, the phase changes are quite obvious to be noticed. Figure 7(b) presents the maximum phase change distribution with the values ranging from 5.0506 rad to −4.8682 rad.

Diffraction patterns were also recorded in a changing environment while using a screen to divert the air flow off the facilities. Figure 8 presents the amplitude distributions of $T(x', y')$ and the corresponding phase changes before the condenser lens obtained from consecutive diffraction patterns recorded with a time interval of 1 s. We find that there are some

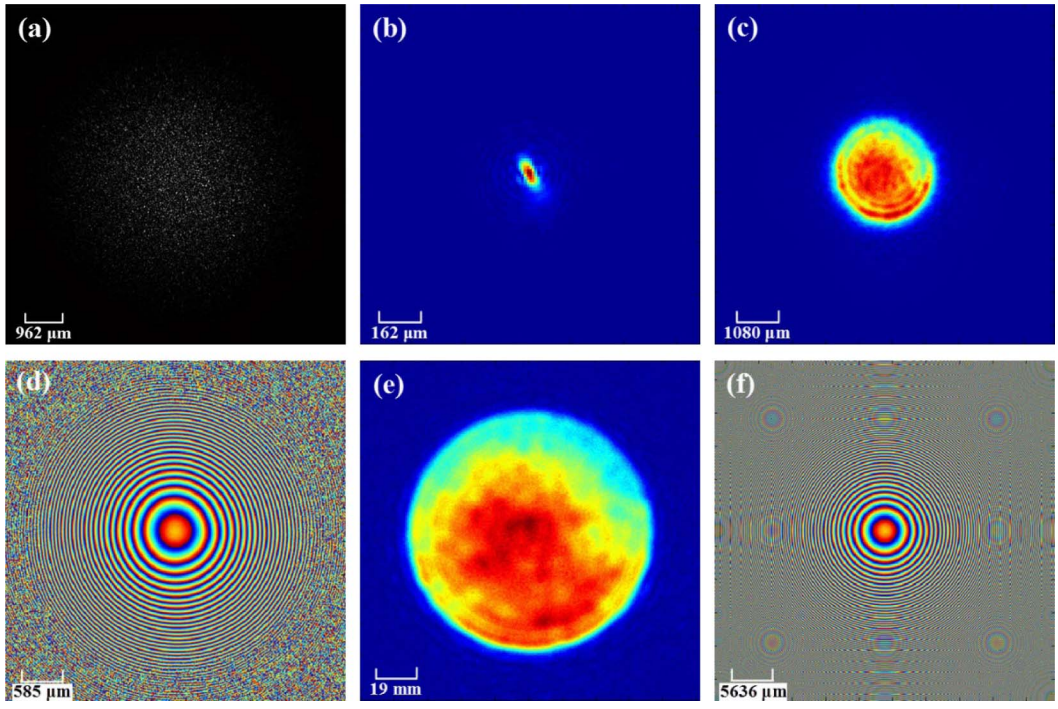

Fig. 4. Recorded diffraction pattern and field reconstructions for the initial stable field. (a) The diffraction pattern recorded by CCD, (b) reconstructed amplitude distribution on the focal plane, (c) reconstructed amplitude, and (d) phase distribution of illumination on the RPP. (e) Numerically obtained amplitude and (f) phase distribution $U(x', y')$ after the condenser lens.

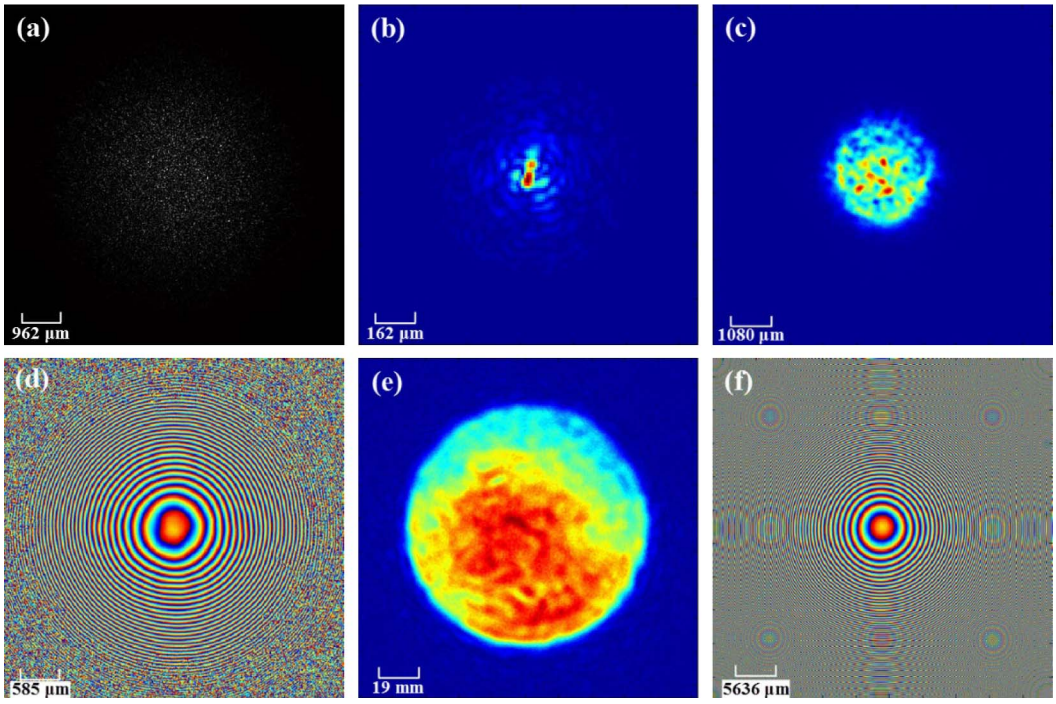

Fig. 5. Recorded diffraction pattern and field reconstructions in a changing environment. (a) The diffraction pattern recorded by CCD, (b) reconstructed amplitude distribution on the focal plane, (c) reconstructed amplitude and (d) phase distribution of illumination on the RPP, and (e) numerically obtained amplitude and (f) phase distribution $T(x', y')$ after the condenser lens.

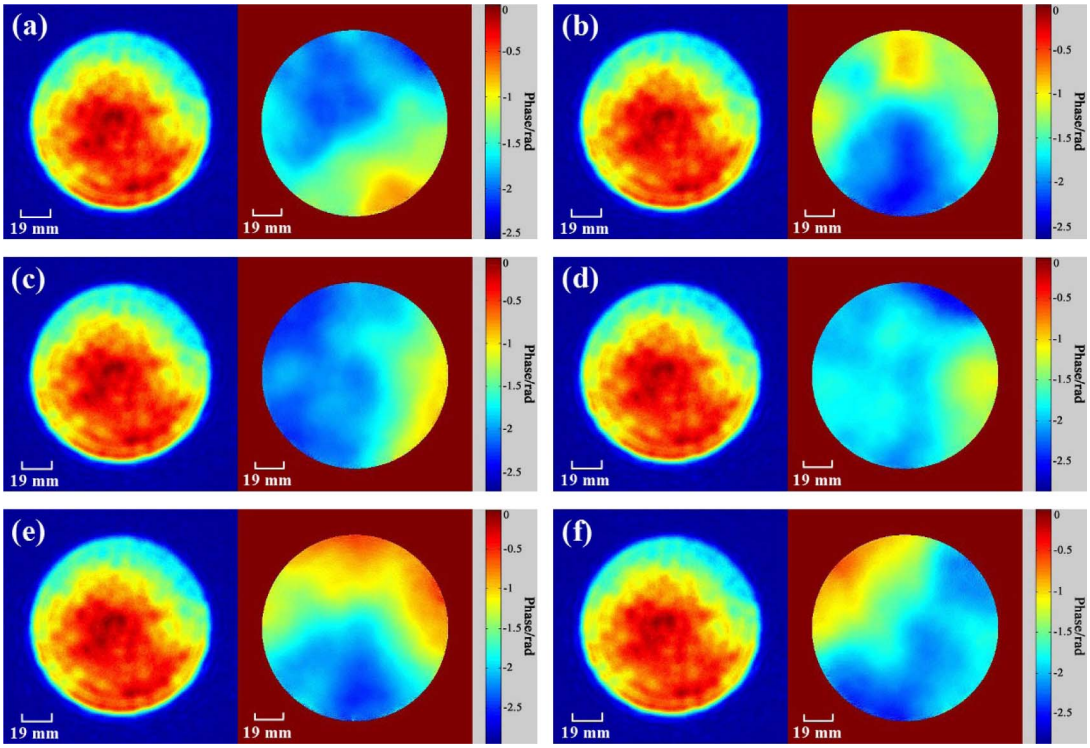

Fig. 6. Series of amplitude distributions of $T(x', y')$ and the corresponding phase changes calculated for large-diameter laser beams which are obtained from diffraction patterns recorded with a time interval of 1 s during the initial stable field.

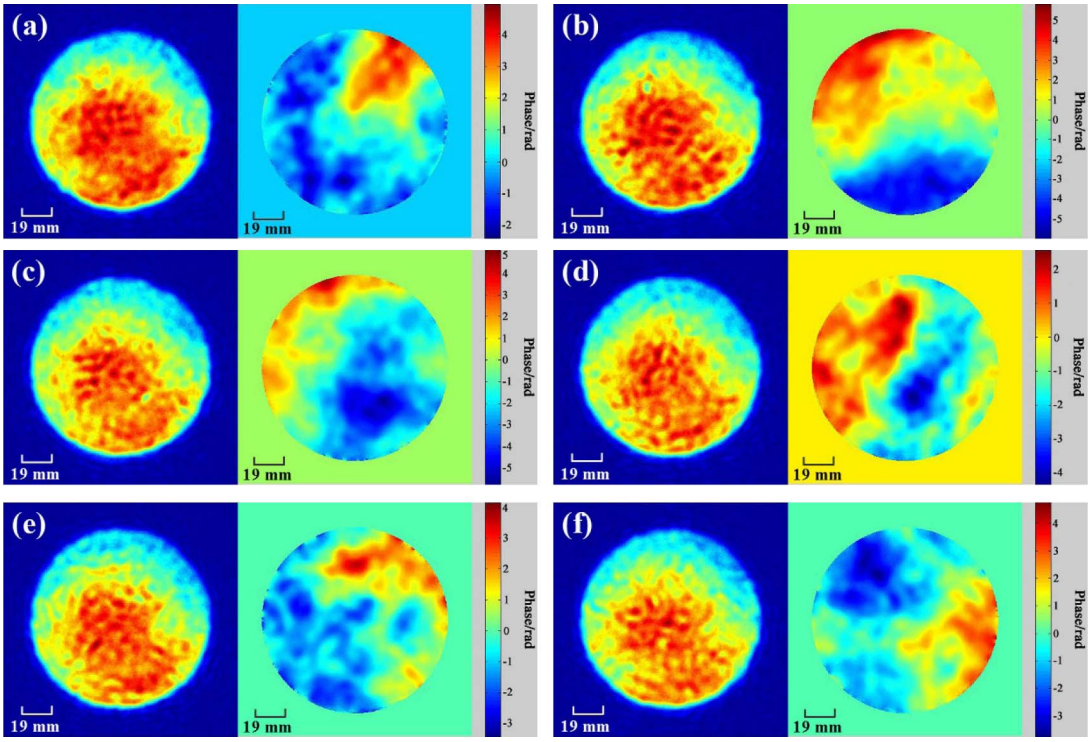

Fig. 7. Series of amplitude distributions of $T(x', y')$ and the corresponding phase changes calculated for large-diameter laser beams which are obtained from diffraction patterns recorded with a time interval of 1 s in a changing environment when the air conditioning is turned on and the air outlets are opened.

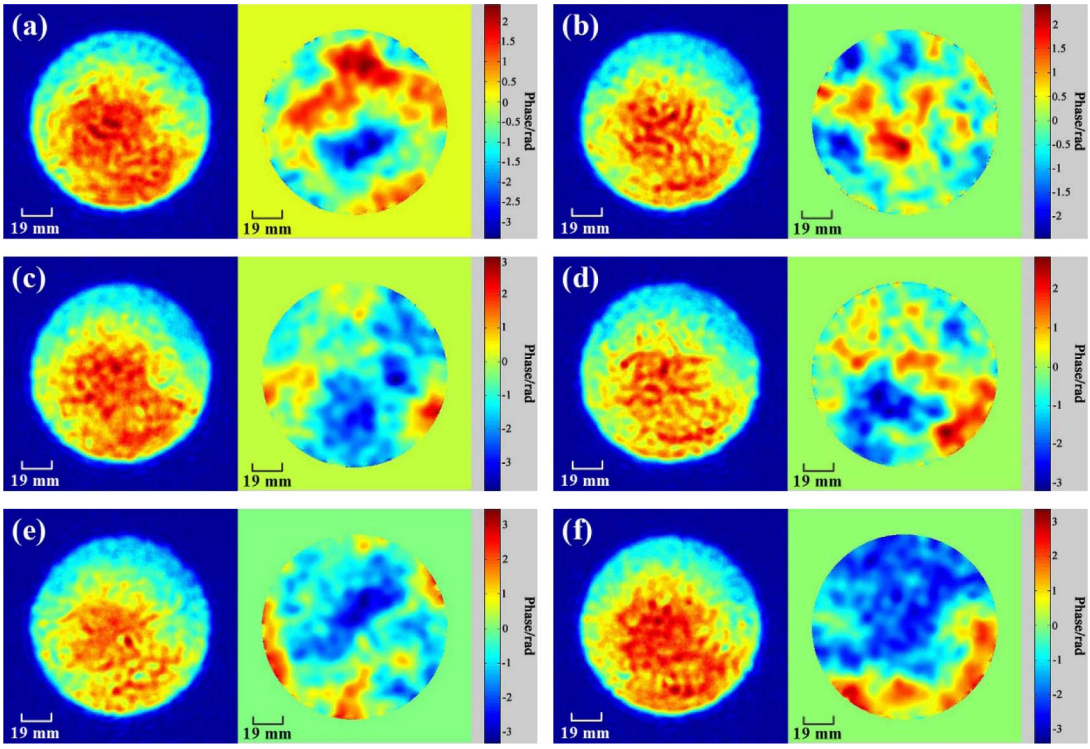

Fig. 8. Series of amplitude distributions of $T(x', y')$ and the corresponding phase changes calculated for large-diameter laser beams which are obtained from diffraction patterns recorded with a time interval of 1 s in a changing environment while the air conditioning is turned on. In this case, a screen is used to divert the direction of air flow from the facility.

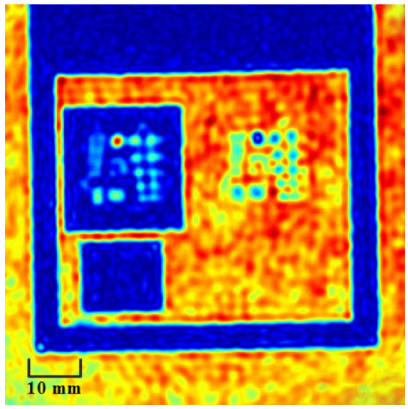

Fig. 9. Transmittance distribution obtained for a USAF 1951 target by the MCI method. It gives a satisfactory resolution in the case of large-diameter beams.

minor changes for the amplitude distributions of $T(x', y')$ with fewer detrimental changes in phase. Figure 8(f) presents the maximum phase change distribution with the values ranging from 2.9208 rad to −2.7395 rad. Comparing the range of values shown in Fig. 8(f) to that shown in Fig. 7(b), it is easy to find that the phase change becomes less obvious. It is demonstrated that the influence of the air conditioning system on the laser beam quality in the high-power facility can be remarkably suppressed by using a screen by diverting the air flow off the facilities.

Since commonly used techniques have their limitations on the measurements of the phase change occurring in large-diameter laser beams in high-power laser facilities, the proposed MCI method can quickly obtain the phase change distribution. The calculation of dynamic phase change is also fast and it lasts only a minute with the MCI method. The result of measuring the laser beam dynamic phase change on-line in a changing environment when the air conditioning is turned on and the air outlets are opened is vividly shown in Visualization 1 (Multimedia view).

The achievable resolution of the phase change distribution of laser beams retrieved by the outlined MCI method is studied by placing a USAF 1951 target before the condenser lens. The transmittance distribution obtained is shown in Fig. 9. This clearly shows a resolution which is about 1 mm. It is a satisfactory result in cases involving such large-diameter laser beams.

4. CONCLUSION

To show and evaluate the influence of the air conditioning system on the laser beam quality in the high-power laser facility, the MCI technique is applied to measure the dynamic phase change of the large-diameter laser beams that is induced by the air fluent and the mechanic vibrations. From the experimental result we can directly find that when the air outlets are closed, the phase of the laser beam is very stable, and when the air outlets ports are windows are opened, the phase of the laser beam changes remarkably and drastically, and the maximum change can reach $\pi/2$ at some points. However, by using a screen to change the direction of the air fluent that directly blows on the facilities the influence can be remarkably suppressed. Accordingly, we can reasonably suggest that the air conditioning system should be temporarily turned off when the laser beams will shoot out or the structure of the air outlet should be modified.

Funding. Chinese Academy of Sciences (CAS) (29201431151100301, 902012312D1100101).

REFERENCES

1. C. A. Haynam, P. J. Wegner, J. M. Auerbach, M. W. Bowers, S. N. Dixit, G. V. Erbert, G. M. Heestand, M. A. Henesian, M. R. Hermann, K. S. Jancaitis, K. R. Manes, C. D. Marshall, N. C. Mehta, J. Menapace, E. Moses, J. R. Murray, M. C. Nostrand, C. D. Orth, R. Patterson, R. A. Sacks, M. J. Shaw, M. Spaeth, S. B. Sutton, W. H. Williams, C. C. Widmayer, R. K. White, S. T. Yang, and B. M. Van Wonterghem, "National Ignition Facility laser performance status," Appl. Opt. **46**, 3276–3303 (2007).
2. W. H. Williams, J. M. Auerbach, M. A. Henesian, J. K. Lawson, J. T. Hunt, R. A. Sacks, and C. C. Widmayer, "Modeling characterization of the National Ignition Facility focal spot," Proc. SPIE **3264**, 93–104 (1998).
3. D. Homoelle, M. W. Bowers, T. Budge, C. Haynam, J. Heebner, M. Hermann, K. Jancaitis, J. Jarboe, K. LaFortune, J. T. Salmon, T. Schindler, and M. Shaw, "Measurement of the repeatability of the prompt flashlamp-induced wavefront aberration on beamlines at the National Ignition Facility," Appl. Opt. **50**, 4382–4388 (2011).
4. S. B. Sutton, C. D. Marshall, C. S. Petty, L. K. Smith, B. M. Van Wonterghem, and S. Mills, "Thermal recovery of NIF amplifiers," Proc. SPIE **3047**, 560–570 (1996).
5. C. R. Wolfe and J. K. Lawson, "The measurement and analysis of wavefront structure from large aperture ICF optics," Proc. SPIE **2633**, 361–385 (1995).
6. D. J. Trummer, R. J. Foley, and G. S. Shaw, "Stability of optical elements in the NIF target area building," Proc. SPIE **3492**, 363–371 (1999).
7. M. L. Spaeth, K. R. Manes, C. C. Widmayer, W. H. Williams, P. K. Whitman, M. A. Henesian, I. F. Stowers, and J. Honig, "National Ignition Facility wavefront requirements and optical architecture," Opt. Eng. **43**, 2854–2865 (2004).
8. W. Jiang and H. Li, "Hartmann–Shack wavefront sensing and control algorithm," Proc. SPIE **1271**, 82–93 (1990).
9. G. Cao and X. Yu, "Accuracy analysis of a Hartmann–Shack wavefront sensor operated with a faint object," Opt. Eng. **33**, 2331–2335 (1994).
10. V. Y. Zavalova and A. V. Kudryashov, "Shack–Hartmann wave-front sensor for laser beam analyses," Proc. SPIE **4493**, 277–284 (2002).
11. S. Sato, T. Mori, Y. Higashi, S. Haya, M. Otsuka, and H. Yamamoto, "A profilometer for synchrotron radiation mirrors," J. Electron Spectrosc. Relat. Phenom. **80**, 481–484 (1996).
12. X. Liu, Y. Gao, and M. Chang, "A partial differential equation algorithm for wavefront reconstruction in lateral shearing interferometry," J. Opt. A **11**, 045702 (2009).
13. R. A. Zacharias, N. R. Beer, E. S. Bliss, S. C. Burkhart, S. J. Cohen, S. B. Sutton, R. L. Van Atta, S. E. Winters, J. T. Salmon, M. R. Latta, C. J. Stolz, D. C. Pigg, and T. J. Arnold, "Alignment and wavefront control systems of the National Ignition Facility," Opt. Eng. **43**, 2873–2884 (2004).
14. H. Wang, C. Liu, X. He, X. Pan, S. Zhou, R. Wu, and J. Zhu, "Wavefront measurement techniques used in high power lasers," High Power Laser Sci. Eng. **2**, e25 (2014).
15. F. Zhang and J. M. Rodenburg, "Phase retrieval based on wave-front relay and modulation," Phys. Rev. B **82**, 121104 (2010).
16. F. Zhang, I. Peterson, J. Vila-Comamala, A. Diaz, F. Berenguer, R. Bean, B. Chen, A. Menzel, I. K. Robinson, and J. M. Rodenburg, "Translation position determination in ptychographic coherent diffraction imaging," Opt. Express **21**, 13592–13606 (2013).

17. H. Tao, S. P. Veetil, J. Cheng, X. Pan, H. Wang, C. Liu, and J. Zhu, "Measurement of the complex transmittance of large optical elements with modulation coherent imaging," Appl. Opt. **54**, 1776–1781 (2015).
18. X. Pan, S. P. Veetil, C. Liu, Q. Lin, and J. Zhu, "High-contrast imaging for weakly diffracting specimens in coherent diffraction imaging," Chin. Opt. Lett. **11**, 021103 (2013).
19. S.-W. Bahk, J. Bromage, I. A. Begishev, C. Mileham, C. Stoeckl, M. Storm, and J. D. Zuegel, "On-shot focal-spot characterization technique using phase retrieval," Appl. Opt. **47**, 4589–4597 (2008).
20. S. Matsuoka and K. Yamakawa, "Wave-front measurements of terawatt-class ultrashort laser pulses by the Fresnel phase-retrieval method," J. Opt. Soc. Am. B **17**, 663–667 (2000).
21. B. E. Kruschwitz, S.-W. Bahk, J. Bromage, M. D. Moore, and D. Irwin, "Accurate target-plane focal-spot characterization in high-energy laser systems using phase retrieval," Opt. Express **20**, 20874–20883 (2012).
22. J. M. Rodenburg and H. M. Faulkner, "A phase retrieval algorithm for shifting illumination," Appl. Phys. Lett. **85**, 4795–4797 (2004).
23. H. M. L. Faulkner and J. M. Rodenburg, "Movable aperture lensless transmission microscopy: a novel phase retrieval algorithm," Phys. Rev. Lett. **93**, 023903 (2004).
24. A. M. Maiden and J. M. Rodenburg, "An improved ptychographical phase retrieval algorithm for diffractive imaging," Ultramicroscopy **109**, 1256–1262 (2009).